Lumos: An Open-Source Device for Wearable Spectroscopy Research

AMANDA WATSON* and CLAIRE KENDELL*, University of Pennsylvania, USA
ANUSH LINGAMOORTHY, Drexel University, USA
INSUP LEE, University of Pennsylvania, USA
JAMES WEIMER, Vanderbilt University, USA

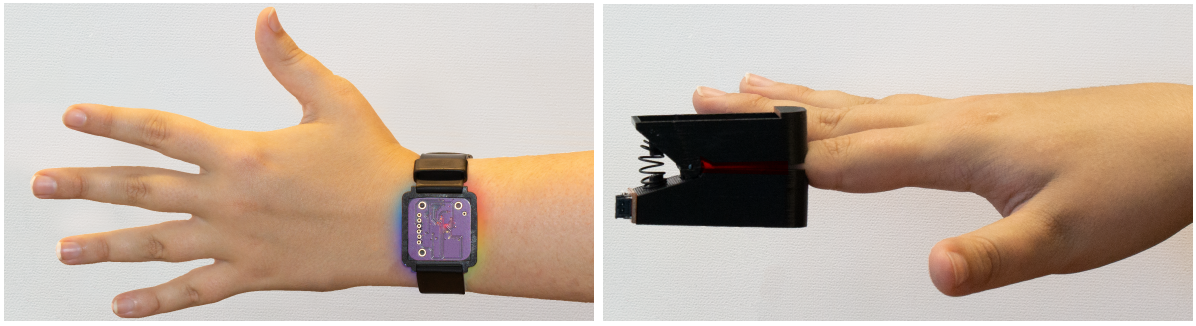

Fig. 1. Lumos is a wearable optical spectrometer that enables non-invasive health monitoring in the real-world. Left: the wristband form factor is familiar and can be worn when moving around in the real-world. Right: the fingertip form factor is more suited to clinic settings and discrete measurements.

Spectroscopy, the study of the interaction between electromagnetic radiation and matter, is a vital technique in many disciplines. This technique is limited to lab settings, and, as such, sensing is isolated and infrequent. Thus, it can only provide a brief snapshot of the monitored parameter. Wearable technology brings sensing and tracking technologies out into everyday life, creating longitudinal datasets that provide more insight into the monitored parameter. In this paper, we describe Lumos, an open-source device for wearable spectroscopy research. Lumos can facilitate on-body spectroscopy research in health monitoring, athletics, rehabilitation, and more. We developed an algorithm to determine the spectral response of a medium with a mean absolute error of 13nm. From this, researchers can determine the optimal spectrum and create customized sensors for their target application. We show the utility of Lumos in a pilot study, sensing of prediabetes, where we determine the relevant spectrum for glucose and create and evaluate a targeted tracking device.

CCS Concepts: • **Human-centered computing** → **Ubiquitous and mobile devices**.

Additional Key Words and Phrases: spectroscopy, wearable technology, health tracking

*Both authors contributed equally to this research.

Authors' addresses: Amanda Watson, aawatson@seas.upenn.edu; Claire Kendell, ckendell@seas.upenn.edu, University of Pennsylvania, USA; Anush Lingamoorthy, Drexel University, USA, aln57@drexel.edu; Insup Lee, University of Pennsylvania, USA, lee@seas.upenn.edu; James Weimer, Vanderbilt University, USA, james.weimer@vanderbilt.edu.

2474-9567/2022/12-ART187 $15.00
https://doi.org/10.1145/3569502

ACM Reference Format:
Amanda Watson, Claire Kendell, Anush Lingamoorthy, Insup Lee, and James Weimer. 2022. Lumos: An Open-Source Device for Wearable Spectroscopy Research. *Proc. ACM Interact. Mob. Wearable Ubiquitous Technol.* 6, 4, Article 187 (December 2022), 24 pages. https://doi.org/10.1145/3569502

1 INTRODUCTION

Spectroscopy, the study of the interaction between electromagnetic radiation and matter, is a vital technique in many disciplines. In medicine, spectroscopy has facilitated substantial advancements in diagnostic technology. Developments in spectroscopy have brought about biomedical imaging technology, including X-ray, MR spectroscopy, and CT scan technology. Additionally, analysis of biological samples relies heavily on spectroscopic techniques to measure the biomarkers that track the progression of diseases. In its current instantiation, its utility is limited because it only provides a brief snapshot of the monitored parameter. Data in isolation, not in a time series, does not provide the trends clinicians rely upon to make informed decisions.

Wearable technology brings sensing and tracking technologies to the masses. Integrating this technology into our daily lives has collected a wealth of previously untapped data. Capturing this amount of data has created longitudinal datasets ripe for analysis. These datasets present opportunities for the application of machine learning and data analytic techniques. This data, combined with machine learning and artificial intelligence, can support clinical decisions, opening the door to more accurate diagnoses. More so, it has transformed how people live, impacting their daily routines, interactions with others, and health monitoring. These qualities make wearable technology the perfect vehicle to collect continuous data from spectroscopy devices.

The traditional benchtop spectrometer is already being minaturized [7, 8, 40, 77]. Sampling and testing are being done in the lab, clinic, and field via portable spectrometers [23, 27, 56, 67]. Optical sensing [17, 58] has demonstrated the viability of a wearable spectral device but is limited by its sensing spectrum. Providing researchers, clinicians, scientists, and even the general public with a more comprehensive wearable spectrometer will increase the amount of meaningful data collected as well as lead to novel clinical applications. Compared to prior work, our approach creates a ready-to-use research platform that can be utilized to develop these novel applications and longitudinal datasets.

In this paper, we address the following research questions:

- RQ1: How can we redesign the traditional benchtop spectrometer while accounting for the many constraints of a wearable device including battery life, computing constraints, and overall footprint?
- RQ2: How can we determine the spectral response of a medium while adapting to dynamic environments given a limited set of light emitting diodes and photodiodes?
- RQ3: How can this device be leveraged to address research challenges in target applications?

The potential benefits of integrating spectroscopy into wearable technology are substantial. In this work, we present Lumos, a wearable spectroscopy device that enables noninvasive, real-time, and continuous health monitoring. To make Lumos available to the research community, we open-sourced the hardware designs and algorithms used in this work [72]. This includes the components, schematics for the circuitry, Gerber files for printing the PCB, and code. We provide the CAD files for the 3D printed form factors, wristband and finger clamp, to house the circuitry. Lumos uses off-the-shelf components that can be combined in the manner we describe in this paper for research purposes or be tailored to fit a targeted application. We evaluated our device on its accuracy when compared with a traditional spectrometer, its power consumption, and its reactions to temperature and fluid.

We developed an algorithm to detect the spectral response of a medium. This determines the optimal spectrum for further evaluation when creating a wearable spectroscopy device for a target application. This algorithm seeks to construct the spectral response of only the medium. It adapts to light leakage from the environment

providing maximal invariance to environmental disturbances. It adjusts its light intensity to standardize readings across skin tone, change in pressure applied to the device, blood perfusion, etc. Additionally, we estimate the theoretical response of our device without a medium to remove the bias from our readings. We evaluate this algorithm on its accuracy, resolution, and resistance to outside sources of noise.

Lumos is an open source device that facilitates wearable spectroscopy research in target applications. To demonstrate its utility in a target application, we conducted a pilot study. In this pilot study, we used the Lumos device in a medical application: prediabetes monitoring. First, we monitored blood glucose via a glucometer and compared it to readings from our device. We used the spectral response estimation algorithm to determine the optimal wavelengths for tracking glucose. Then we created a customized device tailored to those wavelengths and demonstrated that the device could be used to track changes in glucose. While we are not currently able to accurately calculate discrete glucose readings, we can determine the change in glucose over time. This is sufficient to track the progression of prediabetes for our target application.

Specifically, our contributions are summarized as follows:

(1) An open-source device to perform wearable optical spectroscopy research. This device is designed to get researchers up and running quickly in new studies and be easily tailored for custom applications.
(2) An algorithm to estimate the spectral response of a medium to determine the optimal spectrum for a given application while providing maximal invariance to environmental disturbances.
(3) A pilot study, prediabetes monitoring, to demonstrate the viability of using Lumos for a target applications.

The remainder of our paper is structured as follows: Section 2 summarizes the work related to this paper. In Section 3, we introduce the Lumos hardware, including the components used, its form factors, and the underlying theory that supports its operation. Section 4 describes the wavelength algorithm. In Section 5, we evaluate the hardware and our algorithm. Section 6 details our pilot study. Finally, we provide discussion and the future work of this paper in Section 7, and wrap up with our conclusion.

2 RELATED WORK

In this section, we introduce spectroscopy and present how it has been traditionally used as well as how it is evolving. Then, we discuss wearable spectral and optical sensing that has brought heart rate, blood oxygenation, and pulse oximetry to the masses. Finally, we examine applications of wearable spectroscopy that have been studied in the research lab.

2.1 Spectroscopy

Spectroscopy studies the interaction between electromagnetic radiation and matter. It is a vital technique in many disciplines, including medical imaging, molecular analysis, and remote astronomical sensing. The most common types of spectroscopy include atomic spectroscopy [32], ultraviolet and visible spectroscopy [76], infrared spectroscopy [75], Raman spectroscopy [75], and nuclear magnetic resonance [25]. Traditionally, spectrometry, the measurement of the interaction between electromagnetic radiation and matter, is done on benchtop requiring large, heavy, and complex machines with operators that have been specially trained. These benchtop services are characterized by the precision and accuracy of their measurements, but due to the complicated processes, procedures can be time-consuming and inconvenient. Furthermore, these techniques cannot be directly applied to living organisms as normal physiologic functions must be maintained. Hence, samples are obtained from living organisms, but this is not an entirely benign process as it typically requires invasive procedures that cause subject discomfort.

Work has already begun to miniaturize the traditional benchtop spectrometer [7, 8, 40, 77]. Many companies [23, 27, 56, 67] have developed portable spectrometers to bring testing directly into the lab, clinic, and field. Despite this, there is still a need to track real-world, longitudinal continuous data on patients. For example, the most

common issue with pain management protocols is the insufficient treatment of pain with opioids. The reasons for insufficient pain management can be caused by one or more of the following: intolerance of side effects from the medications, desire to minimize medication intake, cost of medication, and external sources of influence [12]. Current techniques for monitoring adherence involve lengthy questionnaires and invasive testing. Whereas a wearable spectrometer could solve this adherence problem by continuously monitoring patient opioid use. Additionally, it could help identify drug diversion, a major concern for clinicians and the Drug Enforcement Agency (DEA) [44]. Further, opioid management during in-patient hospice care is an exceptional clinical challenge [63]. The goal is to provide sufficient analgesia for conditions that can be particularly painful. Balanced against this is the desire for a patient to maintain normal cognitive function. Additionally, during hospice care, the goal is to provide the best quality care while minimizing invasive techniques. Rather than drawing blood samples to monitor a patient's opioid levels, a non-invasive monitor would greatly benefit both the patient and clinician. In addition to the above examples, alcohol, ketones [30], blood pH [4], glucose [18], as well as responsiveness to medical treatment and medications [68] could all benefit from being monitored in a continuous, non-invasive, outpatient manner.

2.2 Other Approaches to Spectral/Optical Sensing

Spectral and optical wearable sensors allow for the continuous sensing of various biomarkers. Some biomarkers are directly measured through the skin by placing an optical sensor on a subject's wrist and sampling the response in a portion of the electromagnetic spectrum. Other biomarkers are more complicated and, in their current state, require the collection of a biofluid before analysis can be completed. The basics of wearable optical sensing involve a light source to introduce light into the body through the skin and a sensor to detect changes in the light due to absorbance and scattering. The most widely available wearable optical sensing devices track a wearer's heart rate and blood oxygenation [17, 58]. Heart rate is obtained by utilizing a single light source and a photodetector to measure small changes in blood volume in the capillary layer. Pulse oximetry leverages a dual light source and photodetector to sense variations in the optical characteristics of hemoglobin during oxygenation and deoxygenation [33, 46, 54, 62]. Additionally, researchers have begun the development of wearable sensors that detect various ions in sweat using a UV light source with a photodetector [3, 6, 48]. This allows for the tracking of ions such as sodium, potassium, and heavy metals, which, when imbalanced, can lead to impaired organ system function. More complex wearable optical sensors take the basics and add a chemical reaction. Optical sensing [31, 43, 69], a sensing method that detects light intensity, has brought progress to the wearable detection and monitoring of pH, electrolytes [39, 43], and glucose[21, 28, 65]. Hyperspectral Imaging is a related form of sensing that extends beyond typical the typical bands of red, green, blue, and has been used in various applications, including HyperCam, to detect spectral variance [22].

2.3 Applications of Wearable Spectroscopy

In research, many forms of spectroscopy have been explored for wearable sensing [75]. Most importantly, near-infrared and functional near-infrared spectroscopy has been utilized for physiologic measurements [9, 74, 75]. Near-infrared spectroscopy (NIR) utilizes the wavelength range from 750-2500 nm of the electromagnetic spectrum and has been commonly used to measure oxygenated and deoxygenated hemoglobin through the skin [75]. Functional near-infrared spectroscopy (fNIRS) uses a subset of the NIR spectrum to sense the oxygenation of hemoglobin [16, 36]. Diffuse optical technologies is a model-based technique for NIR measurement done via continuous-wave, frequency-domain, and time-domain spectroscopy [11, 34, 60, 68]. This technique has been used to measure the concentrations and change of hemoglobin oxygenation, water, and lipids [68]. Here, we will present some applications that are becoming possible due to wearable spectroscopy.

Non-invasive blood sugar monitoring has been an elusive objective. Historically, a blood sample is required to detect the concentration of glucose. This is a painful process that creates a barrier to consistent and effective blood sugar monitoring. NIR spectroscopy, a non-invasive modality, has shown potential for detecting glucose [50]. To date, attempts are complicated and plagued by obstacles such as interfering absorption [75] and motion artifacts. Through our research, we have demonstrated the ability to noninvasively and continuously monitor changes in glucose in limited circumstances.

An increased concentration of lactate indicates insufficient blood flow or excessive metabolism. This can have many causes and even more numerous complications. One example is the end organ damage caused by sepsis. Traditional spectroscopy is excellent at detecting the concentration of lactate in a blood sample. Unfortunately, ascertaining the clinical relevance of a single data point can be challenging as it lacks context. Research into a wearable lactate sensor has shown that the NIR region holds promise for detecting changes in lactate concentrations. Budidha et al. [9] showed that changes of 1 mmol/L of lactate in blood analogous solutions are detectable.

The most studied wearable spectroscopy devices use functional near-infrared spectroscopy to detect brain activity. When a region of the brain is more metabolically active, it has increased oxygen requirements. This is detected and provides use in brain-computer interfaces [74]. Diffuse correlation spectroscopy and speckle contrast spectroscopy are applications of functional near-infrared spectroscopy that have been used to measure deep tissue blood flow [16]. Continuous wave diffuse optical imaging implemented in a wearable device has allowed for the measurement of oxygenation changes in breast tumors during chemotherapy. This device uses six LED and photodiode pairs [68]. Theoretically, this can provide clinicians with the ability to assess the effectiveness of their treatment and modify it in real-time.

Wearable technology provides the ability to simultaneously attach sensors to many areas of the body. This allows for the capture of a diverse set of physiologic characteristics in real-time. Further, it promotes research outside of the lab for situations in which it is unreasonable to use traditional benchtop methods. Spectroscopy is a powerful tool that is essential for analyzing and identifying human disorders. Thus far, it has been an underused modality limited to providing transient snapshots of data. Advances in wearable technology have allowed for the application of spectroscopy techniques to health sensing. Moving forward, wearable spectroscopy provides the opportunity to continuously track the progression of disease or even health of a subject. It creates an opportunity to collect massive amounts of high-value longitudinal data. That amount of data could be used to gain remarkable insights into human health and performance.

3 LUMOS HARDWARE

In this section, we discuss the hardware that makes up the Lumos device. We first examine the theory of spectroscopy and its applications in the wearable domain. Then, we describe the two 3D printed form factors created to house our device. Finally, we discuss the off-the-shelf components and circuitry used to create our device.

3.1 Theory of Operation

Spectroscopy, as previously stated, is the study of the interaction between electromagnetic radiation and matter. It has two main interactions: absorption and emission of photons, particles of light. The measurement of the the photons gives information about the medium [70]. Absorption is when electromagnetic radiation, such as light, is absorbed via a change in energy as it passes through a medium [55]. The wavelengths that are absorbed or partially absorbed would present a lower number of photons at the detector, while the wavelengths that were transmitted would present a higher number of photons. This is depicted in Figure 2a. The figure displays a multicolored light shining on and interacting with a medium. That medium absorbs a portion of the spectrum,

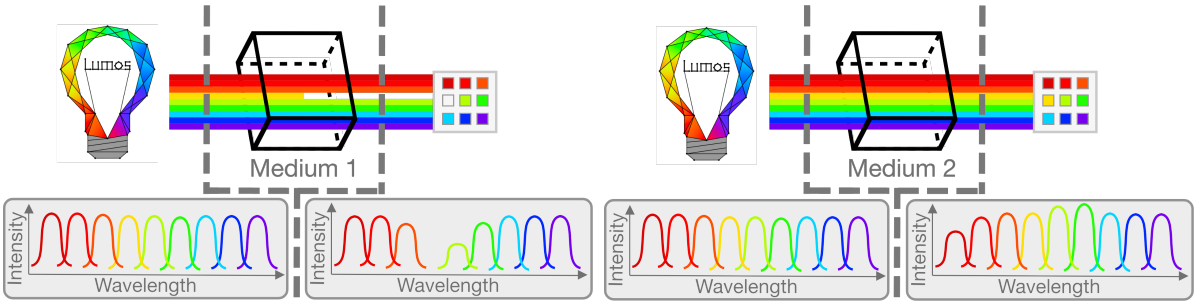

(a) Absorption Spectroscopy

(b) Emission Spectroscopy

Fig. 2. Theory of Spectroscopy

yellow wavelengths. The remaining light is read by the sensor on the opposite side of the medium, showing lower counts at the sensors near the yellow wavelengths. Emission is when the electromagnetic radiation applied to a medium results in the release of photons due to absorption of photons that were applied [42]. This is depicted in Figure 2b. The figure displays a multicolored light with various center wavelengths shining on and interacting with a medium. This medium emits photons which are visible to the human eye as green light when illuminated by the multicolored light. This release, as well as any transmitted light, is captured by the detector. The emission of photons must obey the conservation of energy. Thus, the emmision would not be greater than the energy absorbed. These measurements grant us insight into the medium itself. Mediums can have both absorption and emission occurring at once. Thus, we use this theory as a basis for our sensor and algorithm design in this paper.

Traditionally, optical spectrometers measure the photons either transmitted through a medium or reflected from a medium. Transmission-based spectrometers place the sensor on the opposite side of the medium from the light source. Reflectance-based spectrometers place the sensor and light source on the same side of the medium. Each method has its advantages and disadvantages. To discuss the differences between the two in a wearable configuration, we will use pulse oximetry as an example. Pulse oximetry is a non-invasive application of spectroscopy to monitor oxygen saturation. Studies have shown both transmission and reflection-based devices can provide accurate oxygen saturation measurements [45]. Transmission-based devices, such as the finger clamp commonly used in medicine, are best used in thin areas where the entirety of the medium can be perfused with light. While this limits the on-body locations in which the sensor can be placed and the wearers' movement, this style of sensor is trusted in medical settings. Reflection-based pulse oximetry is generally housed in a smartwatch. It is useful when light cannot fully travel through the medium to show an optical response on the other side [14]. The light source and sensor are placed side by side for reflection-based measurements, which gives more flexibility for on-body locations of measurement [14, 46]. However, light source and sensor alignment are more complicated with this method. As such, a small change in the angle of a surface mount light emitting diode (LED) can drastically change a measurement. As both methods have pros and cons, we seek to incorporate both into our designs. This will require additional data processing as well as separate form factors.

When designing Lumos, we pursued designs that would measure absorption and emission as well as measure photons through transmission and reflectance. Next, we will discuss the form factors we created to make this possible.

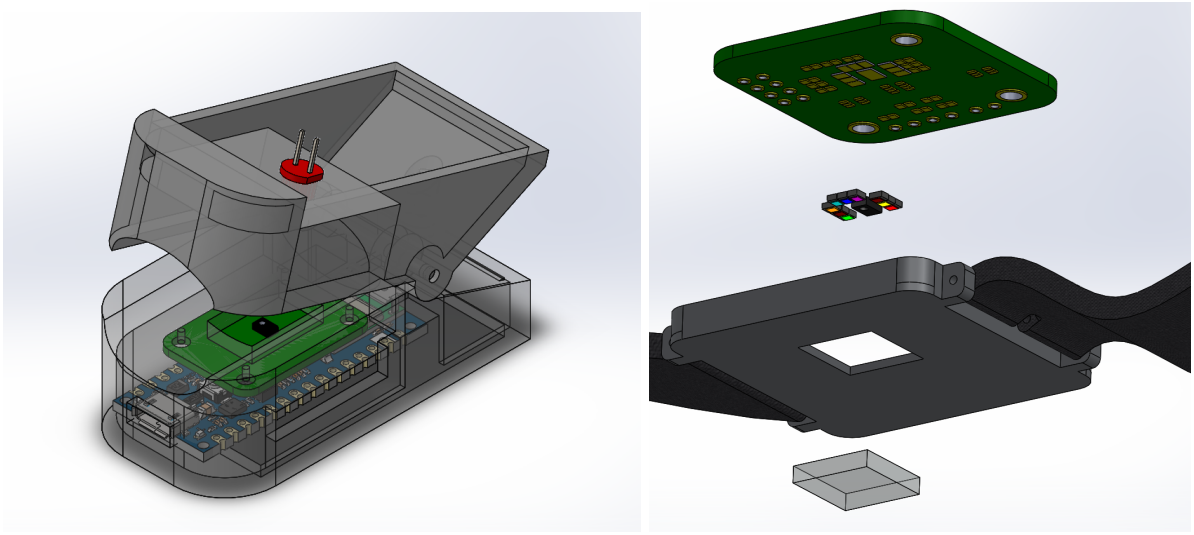

(a) Finger Clamp Form Factor (b) Watch Form Factor

Fig. 3. Lumos Device Form Factors

3.2 Form Factors

As we developed Lumos, we pursued designs already commonly used in wearable technology. This led us to two form factors, a wristband form factor with a similar design to a smartwatch and a finger clamp form factor with a similar design to a pulse oximeter. These designs are shown in Figure 3. The finger clamp leverages transmission spectroscopy and places the light source on the opposite side of the medium from the detector. The wristband leverages reflectance spectroscopy by placing the light source and photodetector on the same side. Both the wristband and finger clamp allow for emission and absorption spectroscopy based on the spectrum input. These form factors offer users a more comfortable experience when using our devices. Furthermore, as they are mainly 3D printed, with a few additional easy-to-find components, they do not require a large time or resource investment. The 3D print schematics are available on our Github [72] with links to the auxiliary components such as springs and pins that were used.

3.2.1 Finger Clamp. The first form factor is the finger clamp, and it is shown in Figure 3a. It is similar to commercially available pulse oximeters in that it rests on the distal phalanges of the finger. This form factor was chosen because it is comfortable, easy to use, and generally familiar to people. It leverages transmission spectroscopy in which light shines on one side of a medium, with the detector on the other side reading the photons from absorption or emission. The finger clamp consists of the 3D printed housing, a spring to keep the housing closed, and a bevel pin to open and close around. When designing this form factor, we addressed two main challenges: consistent pressure from the clamp without causing discomfort and light leakage from the environment. Consistent pressure is needed because as pressure varies, the measurements also fluctuate. So, we introduced a spring and pin to standardize the amount of pressure applied while remaining comfortable to the wearer. Light leakage is the environmental light sensed by the detector. If too much light leaks in, it can obscure subtle changes in our measurements. To address this, we closed off the sides of our form factor as shown in Figure 3a. Additionally, through hole or surface mount LEDs can be used in this form factor.

3.2.2 Wristband. The second form factor is a wristband, as shown in Figure 3b. This is similar to a smartwatch in how it rests on the wrist. It has the advantages of being familiar to the user, comfortable, and can be worn all day. The wristband form factor is based on reflectance spectrometry, so the light source and detector are on the same side of the medium. Because of this, we are less limited in the locations this sensor can be placed. For example, if we extend the straps, it could be attached to the upper arm or leg. This form factor consists of the 3D printed housing, straps, and a skin-safe encapsulant. The skin-safe encapsulant separates the electronic components from the skin, which is essential in a wearable device. It is a transparent silicon that provides a moisture barrier from any sweat on the skin. The entire assembly protrudes from the bottom of the wrist band to ensure tight contact with the skin. Additionally, this encapsulant allows for the device to be worn tightly on the skin, decreasing the amount of light leakage and standardizing the amount of pressure applied.

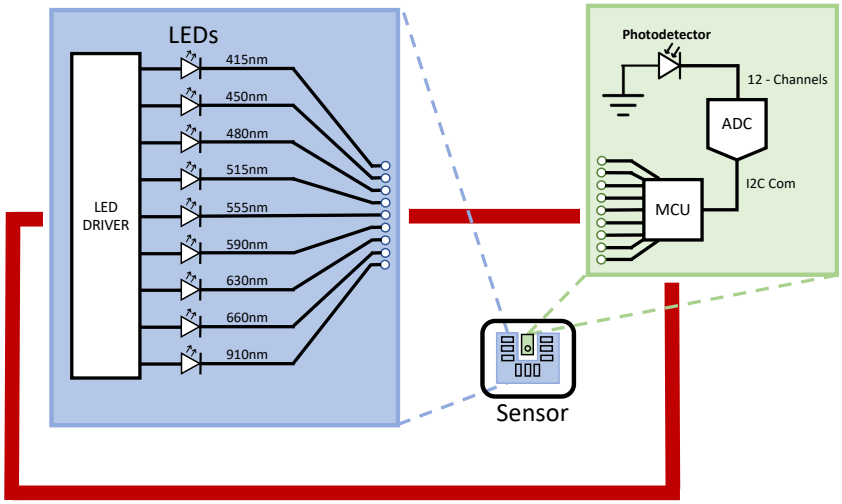

Fig. 4. Block diagram of Lumos Device. The surface mount LEDs generate light and the photodetectors read the light through a medium. These readings are sent to the controller board, where the ADC samples the data and communicates it to the collection system.

3.3 Components

Both form factors described above are based on the same electrical components; they are housed in different configurations. At a high level, the Lumos device consists of a light source and a detector. The light source we describe includes commercially available surface mount LEDs that cover the entire visual spectrum and LED drivers to control the intensity of the light. The LEDs are configurable based on the spectral needs of the application. The detector consists of the sensor with the spectral sensor, microcontroller, communication component, and battery. To house these electronics, we developed a small custom printed circuit board (30mm x 30mm x1.6mm) to ensure a small footprint to fit into our form factors. Figure 4 shows the component diagram for our device.

3.3.1 Light Source. The goal of the light source is to cover the targeted spectrum and appropriately illuminate the medium. This is accomplished through an array of surface mount LEDs and LED drivers. In the finger clamp, the light source sits on top of the form factor. In the smartwatch, it is integrated into the same printed circuit board (PCB) as the photodetectors.

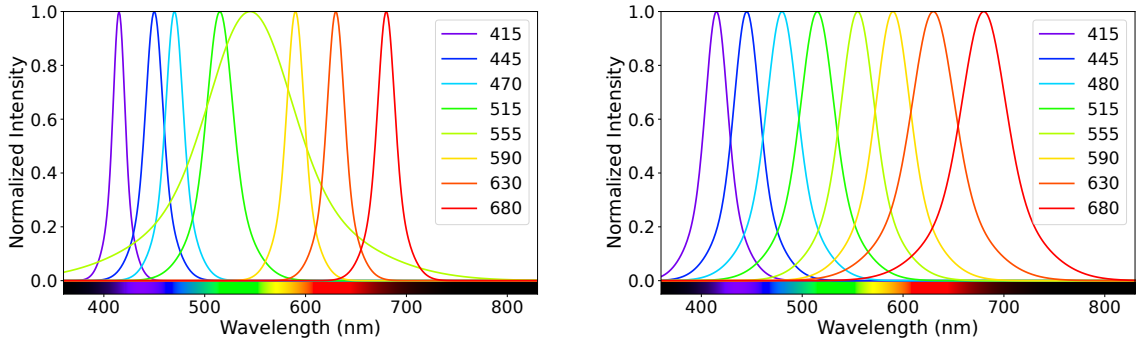

(a) LED Wavelengths

(b) PD Wavelengths

Fig. 5. Spectral Response of our LEDs and PDs

To build a comprehensive system, in this paper, we selected an LED array that covered the visual spectrum. Each LED [53] produces light in a continuous spectrum centered around one peak wavelength. We have eight LEDs in the visual spectrum with center wavelengths around 415nm, 450nm, 470nm, 530nm, 568nm, 599nm, 633nm, and 660nm. The LEDs do have spectral ranges that overlap. This is shown in Figure 5a. In this figure, the total spectrum covered is shown as well as the overlap between LEDs. To handle the complexity that the overlaps may cause, we developed an algorithm that we will discuss in detail in Section 4.

To appropriately perfuse the medium, we use LED drivers to tailor the intensity of each LED. This is important so that the intensity of the LED is high enough for a meaningful measurement but not too high that it will oversaturate the photodiode. The LED drivers also allow us to have consistent readings between all LEDs. We will provide more information on the intensity calibration algorithm that we use to tailor the intensity of each LED in Section 4.

3.3.2 Detector. The detector senses the response from the light source applied to the medium. It consists of the spectral sensor, microcontroller, and communication component. The spectral sensor is integrated into our custom PCB. The microcontroller and communication component are housed on a separate board.

We chose the A7341 spectral sensor [2] because it has a large sensing range and can easily be integrated into a wearable device. It has eight channels in the visible range, with peaks centered around 415nm, 445nm, 480nm, 515nm, 555nm, 590nm, 630nm, and 680nm. The sensing channels are displayed in Figure 5b. The dimensions of this device are 3.1mm x 2mm x 1mm. Thus, it fits into our form factors nicely, as shown in Figure 3a and Figure 3b. The AS7341 needs 1.8VDD for operation. The max current draw from the AS7341 is 300µA making it low power. We will evaluate the power consumption as well as battery life in Section 5.

We chose the Arduino Nano 33 IoT to power our AS7341 and communicate data from the AS7341 to the data collection system. The Arduino Nano 33 IoT has a Cortex M0+ SAMD21 processor and NINA-W102-00B WiFi/BLE Module. It has the ability to send data out over WiFi using MQTT to the data collection platform [73] as it eliminated our need for an additional device such as a smartphone to route the data to the data collection system. The Arduino and the entire device are powered by a 400 mAh lithium-ion battery. This gives it approximately five hours of battery life with an evaluation of this in Section 5. The Arduino supplies 3.3V, which is more than needed for our spectral sensor. As such, there is a voltage regulator on the AS7341 so the Arduino can safely power the spectral sensor. In future iterations of this prototype, we will be looking to shrink this chip to be more compact and tailored to our device, as this Arduino is excessive. This will lead to reduced power consumption and overall space footprint.

4 SPECTRAL RESPONSE OF MEDIUM

In this section, we detail the algorithm used to determine the spectral response of a medium. This allows us to target that spectral response for a specific application, increasing battery life, decreasing computation requirements, and reducing the overall footprint. First, we need to calibrate the intensity of our LEDs to account for environmental light, skin tone, change in pressure applied against the device, and blood perfusion. Second, we eliminate environmental light leakage. Third, we remove the reading we theoretically expect to see if there was no medium. Finally, we identify the spectrum of interest we should target moving forward.

4.1 Intensity Calibration

LED light intensity is affected by many factors, including environmental light, skin tone, change in pressure applied against the device, and blood perfusion. To remove the impact of these factors, each LED's intensity is calibrated for each person and environment. This one-time calibration process occurs when the user first puts it on. It takes approximately 2-5 seconds to calibrate each time. The calibration process is necessary to mitigate over and under saturation on the detector side. Overall, the calibration process adjusts the light intensity until a targeted reading is obtained at the photodetector. We calibrate each LED's brightness on the photodetector nearest to its wavelength. For example, the 470nm LED will be calibrated with the 480nm PD.

Our photodetectors have a 16-bit resolution giving us a maximum value of 65,535. To leave room to sense both absorption and emission, we choose a target value of approximately $\frac{2}{3}$ of our maximum reading or between 42,000 counts and 44,000 counts. This gives our sensor a higher sensitivity while leaving ample room for emission readings. This can be adjusted based on the needs of the application. The iterative calibration process is performed by adjusting the current to the LED using an 8-bit LED driver that adjusts the light intensity until it reaches our targeted value. This adjusts the LED with a resolution of 0-255, approximately 0-50mA. At each iteration (i), we calculate the error between the targeted reading (r_t) and the current reading (r_i). A proportional controller is then used to determine the adjustment required for each LED to achieve the desired count value. A proportional gain (K_p) is used to determine the ratio of output response to the error signal. At each iteration, we calculate the intensity (I) with the following equation

$$I_{i+1} = K_p(r_t - r_i) \tag{1}$$

Then after the new intensity is calculated, we adjust the LED and repeat the process until the targeted reading is reached. In general, the entirety of this iterative process occurs in approximately 2-15 iterations or 3-5 seconds. We evaluate the accuracy and time needed to run the intensity calibration in Section 5.

4.2 Environmental Light Leakage

The intensity calibration accounts for the initial environmental light leakage, but as environments change, so does the light leakage. To handle this dynamically, we sample our sensor in two LED states: ON and OFF. When the LED is ON, we read the combination of the spectral response of the medium and the environmental light leakage. When the LED is OFF, we only read the environmental light leakage. The time spent in an ON state is determined by each LED's rise time and the integration time of each of our PDs. The rise time is the time it takes for the LED to reach maximum intensity based on the current calculated in the intensity calibration. The integration time is the amount required for each PD to record a reading. The rise time and integration time are gathered from the datasheets. Then, to eliminate the environmental light leakage from our reading, we take the average of the two OFF states that surround an ON state and subtract that from the ON state. This is done for every PD for each LED.

4.3 Theoretical Approximation

To determine the spectral response of a medium, we compare the readings from Lumos to the expected readings if no medium was present. To do this, we approximate the readings from Lumos if there is no medium. This requires an approximation for each combination of LED and PD. To approximate each combination, we first estimate the spectral response of each component as a Gaussian. Second, we calculate the expected spectral response of each combination. Finally, we adjust our theoretical approximation to account for leakage current.

4.3.1 Gaussian Estimation. Theoretically, the spectral response of our LEDs and PDs are approximately a Gaussian [47]. To estimate the Gaussian, we need three metrics: intensity, center wavelength, and full width half maximum. The intensity (I) is gathered from the intensity calibration step described above. The Gaussian estimation will be scaled to the calibrated intensity. The center wavelength and full width half maximum are available from the datasheets accompanying each LED and PD. The center wavelength (CW), is the wavelength at which the LED or PD is at maximum intensity. The full width half maximum ($FWHM$), is the width of the spectrum at half of the full intensity. When calculating the Gaussian, the $FWHM$ relates to the standard deviation σ by $FWHM = 2\sigma\sqrt{2\ln 2}$. Then, we estimate the spectral response (SR) via the following equation:

$$SR = Ie\exp\left(-\frac{(x-CW)^2}{2(\frac{FWHM}{2.35})^2}\right) \tag{2}$$

The estimated curves for all LEDs are shown in Figure 5a and for all PDs are shown in Figure 5b.

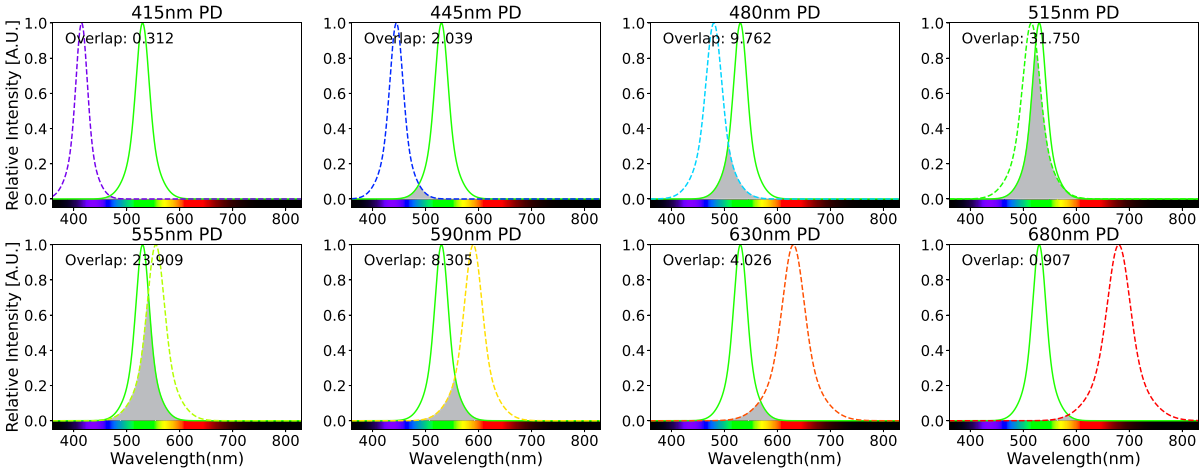

Fig. 6. Calculation of Theoretical Approximation for 530nm (Green) LED

4.3.2 Spectral Response Calculation. Next, we calculate the expected response for each combination of LED and PD. To do this, for each LED, we overlay each PD. In Figure 6, we show this example for the 515nm LED. This LED is shown with each PD, giving us eight graphs. When the LED and PD overlap, we expect a spectral response from the Lumos device. In Figure 6, we see that the LED overlaps with the 445nm, 480nm, 515nm, 555nm, 590nm, and 630nm PDs. For each overlap, we calculate the area under the overlap of the two curves to determine the expected response of each PD. This is normalized to the total possible response from each PD, i.e., the area under the PD curve. We show the estimated responses for the 515nm LED in Figure 7a. Then, we scale the estimated

response to the counts we read from the Lumos device, also shown in Figure 7a. In total, for the eight LEDs and eight PDs, we calculated 64 expected responses.

4.3.3 Leakage Current Adjustment. Photodetectors are not perfect and a known issue is that they produce a leakage current when any photons excite the photodetector [71]. This causes small readings in channels that are not being excited. The readings are linearly related to the number of photons hitting the sensor, i.e., as more photons hit the sensor, the higher the readings. We take an experimental reading without a medium to calculate the leakage current adjustment. We look to the PD readings where the estimated response is zero and average them. This average becomes our current leakage adjustment which is added to all theoretical estimations where the estimated response is zero. This is shown in Figure 7a.

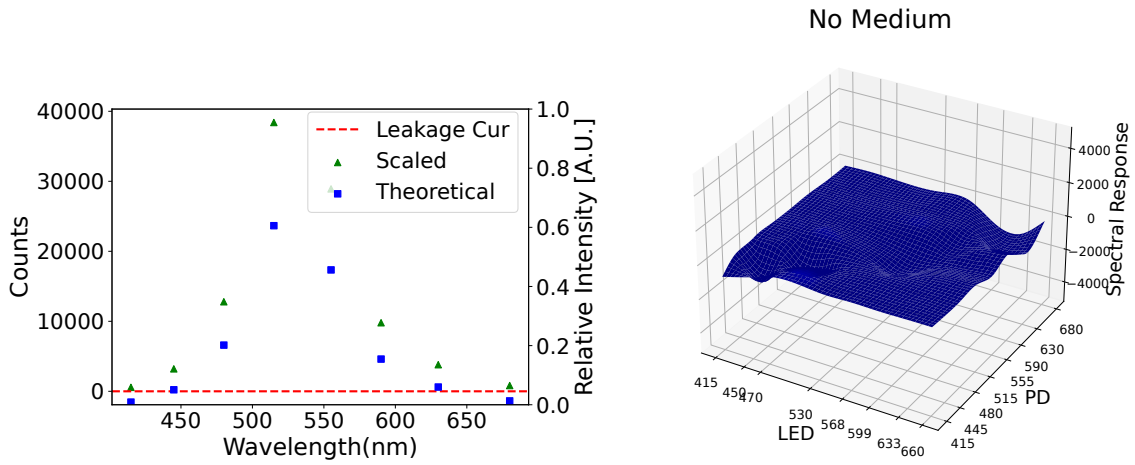

(a) Scaling and Leakage Current Adjustment at 515nm LED

(b) Spectral Response of No Medium

Fig. 7. Spectral Response Calculation

4.3.4 Overall Spectral Response. Finally, we calculate the spectral response of the medium by combining all the PD readings from all of the LEDs. We show the overall response of air or no medium in Figure 7b. The overall response is represented by the entire surface in the figure. The peaks and troughs represent wavelengths with high responses that should be targeted for higher resolution sensing. Peaks represent absorption wavelengths, while troughs represent emission wavelengths. In this figure, we see very little response, which is expected as it is the spectral response of air. We evaluate various mediums in Section 5.

5 EVALUATION

In this section, we evaluate the Lumos Device and the spectral response algorithm. First, we analyze our device. We begin by evaluating its response to temperature and fluids. Then, we examine its power requirements. Then, we compare it to a benchtop spectrometer. Second, we explore the results of our spectral response algorithm. We evaluate the time required for the intensity calibration. Then, we determine the accuracy of our device as compared with mediums with known spectral responses.

5.1 Temperature Experiment

Temperature can affect sensor readings even when not outside of the normal operating range [35, 64]. To understand the effect of temperature on our device, we evaluated the sensor's response to hot and cold temperatures. The sensor, AS7341, is guaranteed to work within the range $-30°C$ to $70°C$. Since we do not expect our sensor to experience the extremes of this range when worn on the body, we evaluate our device between $0°C$ and $45°C$. These temperatures were selected as they are on the edges of normal environmental conditions [59]. For any wearable device, it is important that it withstand normal environmental conditions that humans experience.

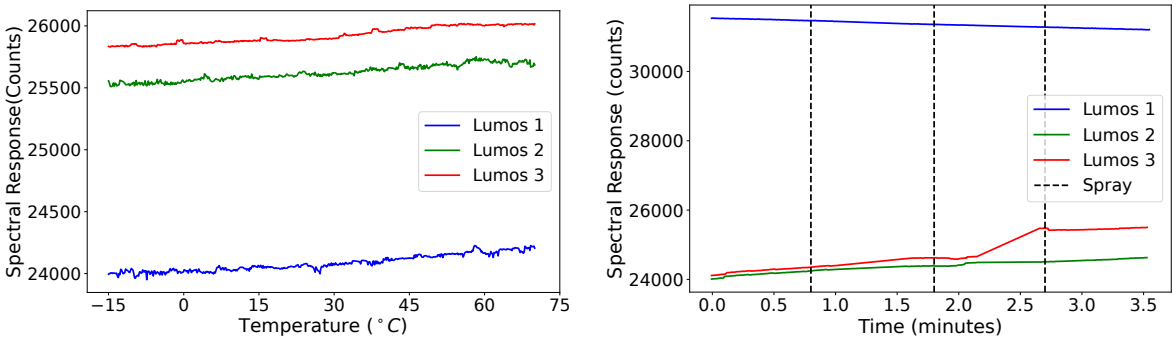

(a) Results from Temperature Experiment

(b) Results from Fluid Experiment

Fig. 8. Temperature and Fluid Experiment Results

To evaluate our device in varying temperatures, we chose a narrow spectrum light source (445nm) that would illuminate a single channel. We tracked the counts on that channel as we varied the temperature between $0°C$ and $45°C$. This experiment was performed with our sensor in a black box to minimize ambient light. To increase the temperature, we used a hair dryer to blow hot air through a hole in the side of the box while not increasing the ambient light. To decrease the temperature, we put the black box into a freezer. In both scenarios, we tracked the temperature with a thermometer. Furthermore, we repeated this experiment across multiple devices to show inter-device repeatability.

We display the results from the experiment in Figure 8a. We show the main channel (445nm) from three devices. The other channels had low counts that did not have noticeable changes related to temperature. The three devices all read the same LED but, due to their placement, received different numbers of photons. This accounts for the difference in counts between the devices. Over the $90°C$ temperature change, we saw a less than 200 count change in our readings on any of the devices. This accounts for a less than one percent change in the overall reading. While we do see a change in the counts, it is small enough that it should not affect the performance of our sensor.

5.2 Fluid Experiment

In addition to temperature, fluids can also impact the sensors. For example, sweat can coat the encapsulant, causing differences in sensor readings. To evaluate Lumos's response, we simulated different levels of sweat. We used our wrist band form factor with a waterproof encapsulant to do this. This was done by spraying the encapsulant with water. We repeated this three times to simulate minimally sweaty to very sweaty, with very sweaty being someone dripping in sweat. Each spray was approximately .75 ml. As above, we performed this study in a black box to reduce light leakage. Figure 8b shows the results from the fluid experiment in the 445nm

wavelength. All other wavelengths followed a similar trend. These results show no significant effect, less than 100 counts, on the spectral response readings until the third spray. This puts 2.25 ml of water onto our sensing area, well past what can be expected from sweating.

5.3 Power

We measured the power consumption of the Lumos device using a digital multimeter to measure the power drawn when all LEDs are at max intensity, PDs are sampled at 10Hz, and our communication protocols are functioning as normal. This is the max power draw from our device. With these settings, the Lumos device consumes 85 mA (425mW) of current. This gives us approximately five hours of battery life with a 400 mAh lithium-ion battery. This is more than sufficient for a normal research study. Longer studies are possible with a higher capacity battery. The Arduino Nano IoT is the most power-hungry part of our device. Replacing this with a lighter-weight component would increase the battery life. In practice, our system could sample data less frequently or transmit data to the data collection system at higher intervals. A sleep functionality could also be implemented so that the device, including the LEDs, PDs, and processing circuitry, do not need to be on when not in use. In Section 7 we discuss opportunities to upgrade the hardware, including some that would increase battery life.

5.4 Intensity Calibration

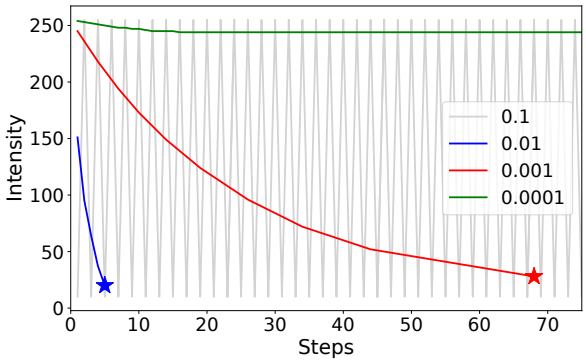

Fig. 9. Intensity Calibration at Each K_p for 530nm LED

To determine the best K_p for our system, we tested four values, $K_p = [0.1, 0.01, 0.001, 0.0001]$. An initial default intensity value of $I = 255$, maximum intensity, was used to start this test. We show the results for how I changed using the 530nm LED at each step for each K_p in Figure 9. The stars show when the calibration algorithm is successfully finished. $K_p = [0.1, 0.0001]$ did not converge to our targeted value even after running for over 100 iterations. $K_p = 0.01$ converged the fastest with an average of 4.8 steps. $K_p = 0.001$ converged in approximately 44 steps. We chose the setting $K_p = 0.01$ for our device as it converged to the targeted value in the fewest number of steps. This took approximately 2.4 seconds. We show the results from each K_p in Figure 1. This setting is adjustable based on the needs of the application. Anything above 0.1 or below 0.0001 does not converge, so we did not test those values.

Table 1. Time and Computational Needs for Each K_ps

K_p	# Steps	SD Steps	Time (s)
0.1	∞	∞	∞
0.01	4.8	2.9	2.4
0.001	44.4	41.3	22.2
0.0001	∞	∞	∞

5.5 Comparison with Spectrometer

In order to validate the AS7341 spectral sensor, we compared it to a ground truth spectrometer, the Ocean Optics Vis-NIR fiber optic spectrometer [52], as seen in Figure 10b. This spectrometer has a range from approximately 450nm to 1118nm with a resolution of 1.37nm. In this study, we generated colors that were similar to what our photodetectors read using an iPad screen. We pointed the iPad at both the ground truth spectrometer and the AS7341 and recorded the readings from both. In Figure 10a, the ground truth spectrometer readings are plotted alongside the AS7341 sensor readings. For the most part, we saw that the AS7341 readings followed the same curve as the ground truth spectrometer and gave confidence in moving forward with this device. We did see more error in the 630nm and 680nm readings. We believe the higher Lumos counts in the red spectrum were due to the PDs on our device having a larger sensing range in that spectrum.

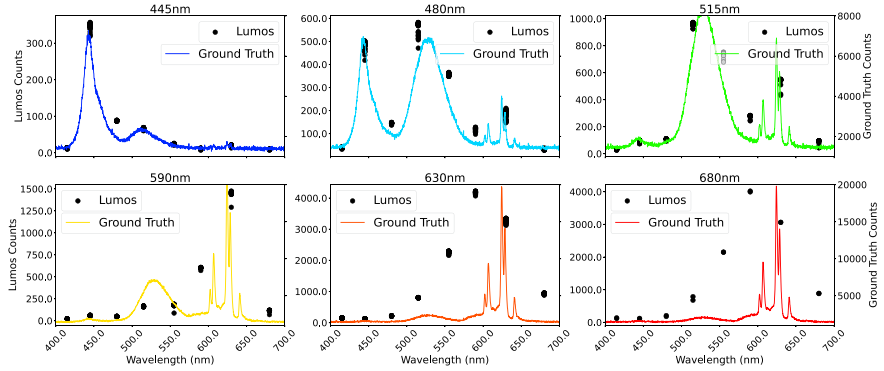

(a) Comparison with Benchtop Spectrometer

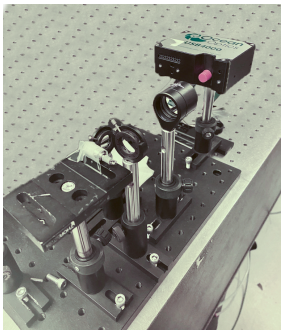

(b) Experimental Setup

Fig. 10. Spectrometer Comparison Experiment

Given the comparisons to the benchtop spectrometer, we see that our sensor does accurately detect the wavelength and intensity of light. However, the limitations of our spectral device are evident. For this study, we selected colors that would match the center wavelength channels of the spectral sensor. However, the color generation for this study was based on hex codes and used a combination of wavelengths to achieve a color [66] which is different than LEDs that are centered around one wavelength. The sensor picked up these combinations but with much less granularity than the ground truth spectrometer. Moving forward from this study, we chose visible LEDs that were centered around a specific wavelength [15, 49, 53, 61]. We understand this device lacks the precision and accuracy of the benchtop spectrometer. However, this iteration of the sensor allows the user to conveniently wear it around the finger or wrist. Additionally, sensing granularity and accuracy can be improved with additional customized hardware which will be discussed in Section 7. The goal of the device was to use

off-the-shelf components to create a wearable sensor that can easily be tailored for research or personal use. We continued with this sensor for our prototype since it met these requirements.

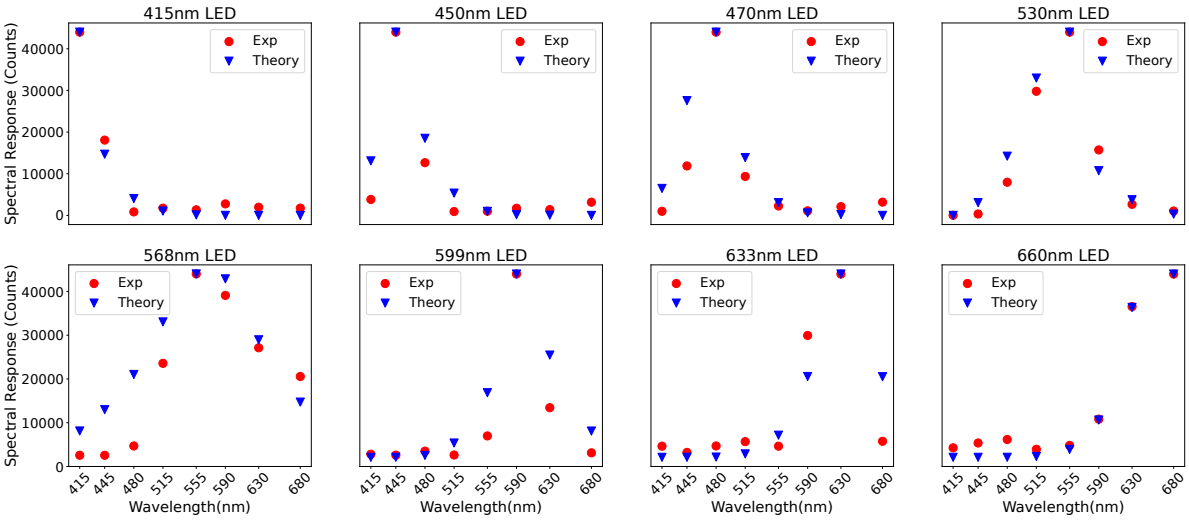

Fig. 11. Comparison of Experimental Measurements and Theoretical Approximation for Each LED

5.6 Theoretical Estimation

We evaluated our theoretical approximation by comparing them to experimental measurements. To record the experimental measurements, we placed the Lumos device in a black box. There were openings in the box for the wires with mitigations to remove all environmental light. We took measurements when the LED was off, and all channels showed zero counts. To have a consistent intensity across all of the LEDs, we used our intensity calibration algorithm to assure 44,000 counts. No medium was placed between the spectral sensor and LEDs. Figure 11 shows the comparison between the theoretical approximations and experimental measurements at each LED. The theoretical approximations have a 0.944 Pearson correlation with the experimental measurements.

5.7 Spectral Response of Medium

We conducted experiments to understand the Lumos device's ability to identify the spectral response of a medium. We started by characterizing the source and detector output with no medium and then moved on to characterize the change in output response when a medium was placed between the source and detector. We consider no medium to be air. The physical mediums we used were six colored light filters: purple, blue, green, yellow, orange, and red. The mediums were placed into the fingertip form factor for this experiment. In order to characterize these, we collected data to show the response of each of our LEDs when measured by all visible photodiode channels for each filter, including with no filter. The algorithm discussed in Section 4 is applied to calculate the spectral response of the mediums or lack thereof. We compare this to the known spectral response of the mediums that we collected from the datasheets.

This experimental data collection was done in a controlled lab setting. The AS7341 spectral sensor was placed in a black box with an LED. The ambient light was mitigated as much as possible. When we took readings with the LED off, all channels showed zero counts. The results of this study are shown in Figure 12. The results from the air medium are shown in Figure 7b. We compared the peaks in these figures to the center wavelengths of the

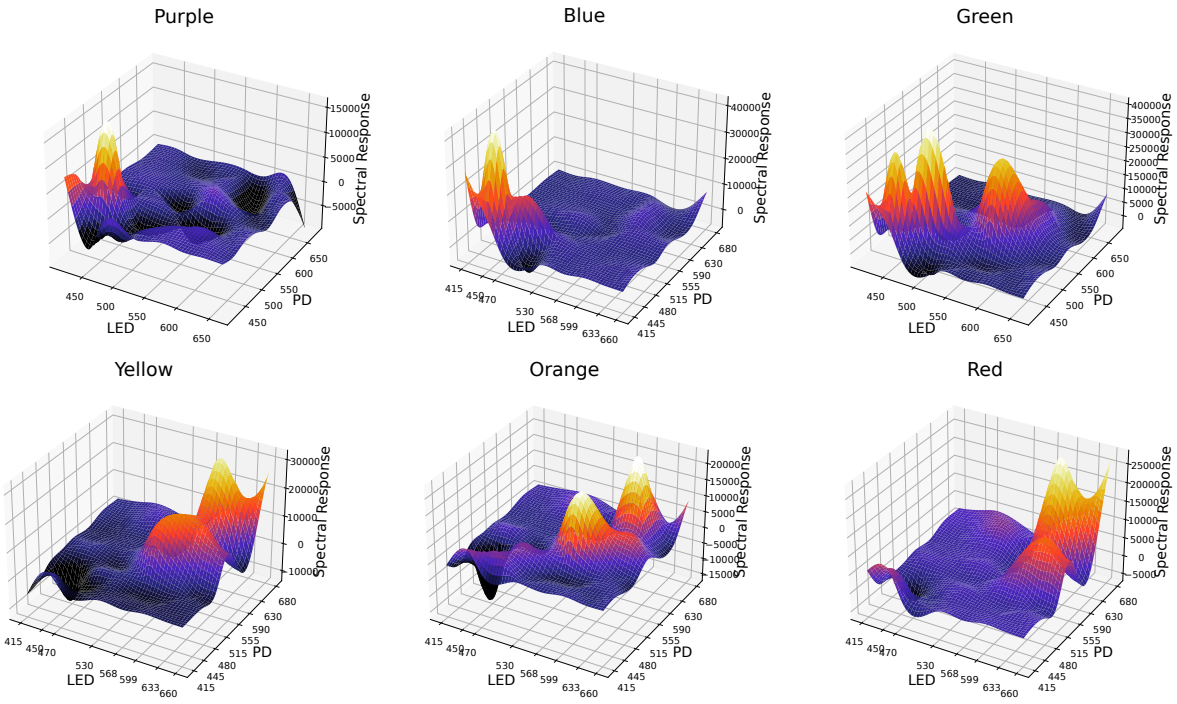

Fig. 12. Spectral Response of Mediums

filters, demonstrating a mean absolute error of 13nm with a standard deviation of 8nm. We further compared this to peak detection before interpolation and showed a mean absolute error of 17nm with a standard deviation of 11nm. Thus, we see that interpolation improves our center wavelength detection. In some cases, the filters, such as yellow, covered the entire spectrum after the initial peak, creating an extended peak. We see our algorithm detect this, but as we do not have a center wavelength to compare against, we removed it from our analysis.

6 PILOT STUDY

Lumos can be used in many different application scenarios, including but not limited to health monitoring, athletics, and rehabilitation. This section discusses a pilot study that demonstrates this, specifically prediabetes tracking. We start by motivating our study and describing the current standard of care in diabetes monitoring. Then, we describe how Lumos facilitated our sensor design and creation. Finally, we evaluate our device and system for accuracy.

6.1 Background and Motivation

Diabetes is a disease that impacts over 400 million people worldwide [51]. It causes a number of complications, including shortened life expectancy, decreased quality of life, blindness, cardiovascular issues, and more. In the United States, over $300 billion yearly is spent to manage and treat diabetes and its numerous complications. Prediabetes is a common precursor to diabetes that is characterized by higher than normal blood sugar levels but lower blood sugar levels than with diabetes [41]. It is possible to treat and even reverse prediabetes through lifestyle changes, but most people with prediabetes are unaware of their condition. To determine if a person

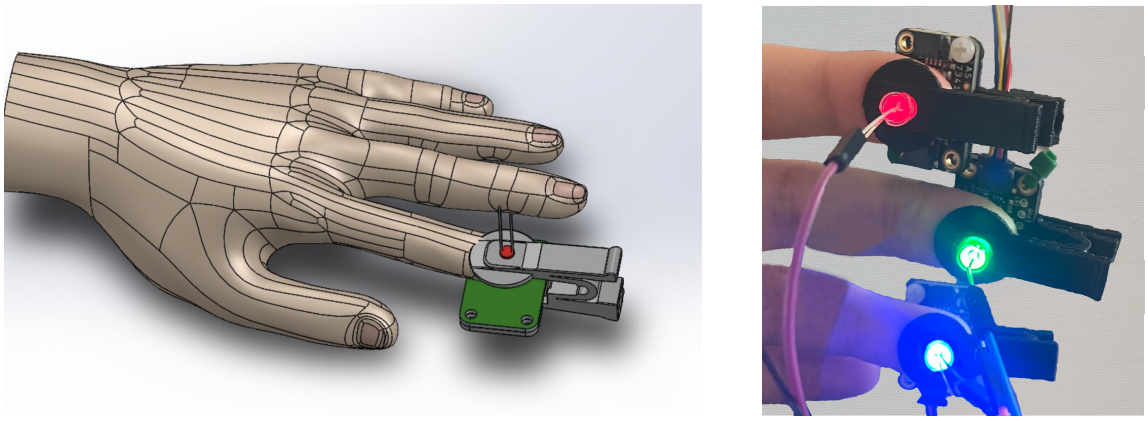

(a) Glucose Form Factor Design (b) Glucose Monitor Prototype

Fig. 13. Glucose Device Design and Initial Prototype

has prediabetes, blood glucose tests are run in the clinic. This process is invasive as it requires drawing blood for accurate measurements. Moreover, it is time and resource intensive creating a barrier to prompt testing. By tracking blood glucose via wearable technology, as well as its overall trends, we can potentially monitor the progression of prediabetes outside of the clinic.

Traditional glucose monitoring requires a blood sample and a glucometer. These monitors have been tested, evaluated, and proven effective for diabetes monitoring and management. New devices have come on the market to try to less invasively monitor blood glucose. Continuous Glucose Monitors (CGM) collect interstitial fluid through a needle inserted into the skin to provide continuous glucose monitoring [51]. Breath Ketone Analyzers estimate glucose levels by measuring the ketones in your breath. Research has begun into less invasive optical methods [1, 24, 29] in the visible [38] and near-infrared range [75] that have been done in lab settings and wearable devices. Specifically, Lepore et al. [38] shows the fluorescence emission of glucose oxidase peaks at around 520nm and increases in the presence of glucose in a lab setting. Dantu et al. [13] found that the ratio of the 510nm wavelength to 475nm wavelength to be an effective metric for tracking glucose. The found that as glucose concentration increases, the ratio decreases, using Beer-Lambert's law. This work was not in a wearable, but using a light source and smartphone. Additionally, 650nm wavelength of light being shown on a solution has been shown to increase in transmittance of photons, with glucose and was done using a handheld device [5]. A noninvasive continuous blood glucose monitor can lead to advancements in timely prediabetes identification. The goal of this study is to demonstrate a proof of concept for such a device by leveraging Lumos.

6.2 Spectral Response Identification

In order to identify the optimal wavelengths to monitor glucose, we ran a preliminary study. In this study, we monitored the glucose of a single person over the course of an hour. This study determined that three wavelengths: 470nm, 515nm, and 680nm, showed promising responses for change in glucose. To validate this, we customized our sensor to target 470nm, 515nm, and 680nm. These wavelengths do not align with the original surface mount LEDs used in Lumos. As these components are different, we developed a new custom form factor shown in Figure 13a. This form factor was designed to house a single through hole LED while maintaining continuous pressure on the finger. Additionally, this form factor is designed such that it can be worn on three fingers simultaneously.

We chose to run each LED on separate fingers to simultaneously collect data from all three sensors without the data loss that switching LEDs could cause. Our prototype is shown in Figure 13b.

6.3 Results

We tested our proof of concept sensor in comparison with a commercially available glucometer [10] in a user study. This study used a single participant where we attached the Lumos devices on the participant's left hand as shown in Figure 13b. The 680nm LED was attached to the pointer finger, the 515nm LED to the middle finger, and the 475nm LED to the ring finger. Blood glucose readings were drawn from the fingers on the right hand. This setup is shown in Figure 13b. Each study was performed over approximately 30 minutes to one hour. We repeated this study five times. Our participant began in a fasted state and we started the studies in the morning. This appears as a low starting glucose readings. When the study began, they drank a sugary drink (soda), and we recorded the effect over time of that on their blood sugar. Approximately every three minutes, we took a new blood glucose reading. We continuously sampled the three Lumos devices at approximately 2 Hz.

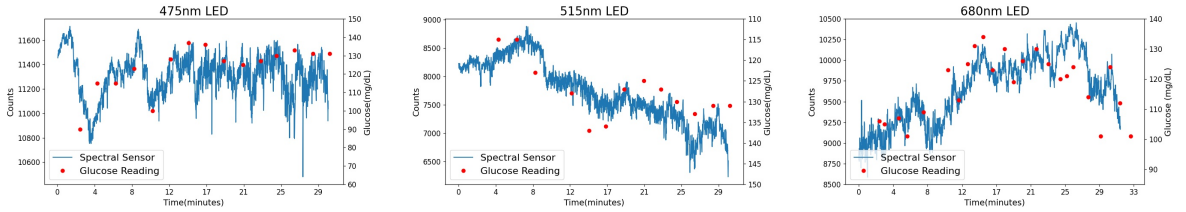

(a) 475nm LED (b) 515nm LED (c) 680nm LED

Fig. 14. Results from Glucose Experiments

In Figure 14 we show the raw data collected from each LED with its targeted PD. The ground truth blood glucose is shown by the red points. It is measured by a commercially available glucometer. The optical spectroscopy readings from the 480nm, 515nm, and 680nm photodetector channels are shown by the blue lines. In Figure 14a and Figure 14c, the change in counts positively trends with the change in glucose. In Figure 14b, the change in counts negatively trends with the glucose readings. In this figure, the y-axis of the glucose readings is flipped. We performed further analysis to quantify the correlations between the glucose measurements and the readings from our sensor at our three target wavelengths. To compare these two data points, we interpolated the missing glucose values using a linear interpolation. We found that 470nm and 515nm were statistically significant with a p-values less than 0.05 and Pearson correlations of 0.843 and -0.927 respectively. The negative correlation showing that the glucose reading and Lumos's reading are highly correlated but in the the opposite directions from each other. 680nm showed relatively low correlation when compared with our ground truth glucose values with a Pearson correlation of 0.359. The lack of correlation for the 680nm channel encourages future work in the surrounding wavelengths including expanding into the infrared spectrum. These results show that readings from our sensor may be used to track overarching glucose trends. They prompt additional research to continue to improve the noninvasive monitoring of glucose and thus track the progression of prediabetes.

7 DISCUSSION AND FUTURE WORK

In this work, we demonstrated Lumos, an open-source device for wearable spectroscopy. It enables real-time, non-invasive, and continuous health monitoring outside of the clinic or lab. We acknowledge that the Lumos device is low fidelity compared to a benchtop spectrometer, but it allows users to determine what wavelengths to target for an application and then build a higher fidelity sensor around those wavelengths. We envision the

Lumos Device being used for research purposes. It is a powerful tool that can help researchers determine the wavelengths of interest for applications. Once the wavelengths have been identified, more targeted devices can be developed. This will help to improve accuracy, battery life, and a form factor can be developed that is suited specifically for the application.

7.1 Device Improvement

While our device provides the ability to perform wearable optical spectroscopy, it is limited in many facets. The size can be decreased and the sensor data can be improved in terms of granularity and overall range. This will be accomplished through customization and miniaturization. Decreasing the size of the device will increase its portability and ease of placement on the body. Increasing the granularity of the device will improve sensing via more data points that will unlock details about the photons being detected with the goal of improving the accuracy of Lumos. Increasing granularity beyond the visible spectrum will bring further insights into the makeup of the medium in other ranges. These works have shown absorption peaks of glucose in the NIR range and we plan to implement this in our work [26, 75].

In order to improve the size of the device, customization is key. This device can be shrunk by swapping the Arduino for a board targeted to our specifications. Beyond that, to further shrink the prototype, a customized circuit could be designed for parts of this system and further tailor our design to our specifications. The next iteration of form-factors for the wrist-based reflective device will include better protection against cross-talk between the LEDs and photodetector. An analysis of the effects of distance and angle between the LEDs and photodetector is needed to determine the optimal placement of components to maximize count values. We also plan to include the frequency and pulse width of each LED as part of the current calibration step to make the device more adaptable to various body compositions while decreasing battery consumption.

The current sensor can only sense eight center wavelengths in the visible spectrum, which reduces the granularity of our device significantly. In the next version of our device, we want to increase this granularity by sensing more center wavelengths along the visible spectrum. We also want to target specific LEDs with a controllable intensity that will be most effective for specific and additional biomarkers and spectrometry technology. Additionally, our current sensor has one specific Near Infrared Reflectance (NIR) channel that it senses, and we want to include NIR sensing in the next version of this device. More than that one channel, we want to expand the sensor beyond the visible range with much more granularity in order to sense more of the electromagnetic spectrum. In expanding the spectrum, both our sensor and source require improvements that span additional wavelengths.

Overall, our current device has potential improvements that will unlock key advancements in the optical sensing of biomarkers in the body. Among these, decreasing the size, increasing the granularity and range, and improving its basic specifications, such as power consumption, will greatly improve the performance and results of the device.

7.2 Algorithm Improvement

Our algorithm details the spectral response of a medium and gives insight into target applications. In this paper, we demonstrated good overall performance of our algorithm. It can be improved in two facets. First, we can continue to improve on the theoretical model. Second, we can upgrade our wavelength detection. Our theoretical approximation approximates the response of a perfect set of LEDs and PDs. In the real world, this is not feasible, and as such, we see errors in our approximations. As there is some error inherently in each LED and PD, we can add additional estimations to account for this error. This will allow for a more accurate approximation. The leakage current bias is currently being calculated based on the experimental reading. This could be modeled and calculated as we calculate the rest of our theoretical response. Each PD should have a baseline leakage

current bias that would then be scaled based on the intensity of the light being shown on our PD. The wavelength detection algorithm finds the peaks of the interpolated data using SciPy. Essentially, if the interpolated data in Figure 12 crosses a certain threshold and is after a certain amount of samples from the previous peak, then a peak is identified and recorded. In order to improve on this, we can detect not only a peak but a range of wavelengths for further analysis. To accomplish this, we should detect a range similar to a full-width half max surrounding the center wavelength where the counts are significant.

7.3 Real World Deployment

The Lumos device has been tested in a lab setting. To further improve our device, we plan to test it in the real world. Lumos will behave similarly to IoT devices, such as smartwatches, by wirelessly collecting signals across multiple wavelengths that can be used to determine biomarkers such as heart rate, respiration rate, blood oxygen levels (SpO2), and glucose. This will facilitate future studies on a broad patient population with varying human physiology, skin pigmentation, and comorbidities. The device has a maximum battery life of five hours with continuous usage of all LEDs. But like many real world deployments, we can duty-cycle the data collection and transfer process. This will significantly increase the battery life and allow longer user studies to be performed. Limiting the wavelengths sampled can also increase the battery life. By collecting data at certain intervals, running the device on low power mode, and limiting the spectrum sampled to what is needed for the study, we can extend the battery life by up to sixty hours, almost twice the amount of a regular smartwatch.

The wrist form factor has the ability to collect data for multiple wavelengths during high-motion scenarios such as running, working out, or playing a sport. To fully utilize this form factor, it needs to be resistant to motion artifacts. Motion artifacts affect specific wavelengths significantly, while others are resistant to them [19, 57]. Testing the various wavelengths we utilize while inducing motion artifacts could help create smarter wearable sensors with adaptable wavelengths depending on the user's state of motion. For example, green wavelengths are more resistant to motion artifacts and have a good signal-to-noise ratio but are easily absorbed by the skin, thereby limiting their penetration depth [37]. Red Wavelengths are great at monitoring heart rate and have deeper penetration than green but are highly sensitive to motion noise [20]. Different wavelengths are also absorbed by the skin differently based on melanin content.

8 CONCLUSION

In this paper, we present Lumos, an open-source device for wearable spectroscopy research. Using our custom PCB and off-the-shelf components, Lumos demonstrates five hours of battery life. We developed an algorithm to determine the spectral response of a medium while remaining invariant to environmental disturbances with a 13nm mean absolute error. From this, researchers can determine the optimal spectrum to target for their application facilitating on-body spectroscopy research in health monitoring, athletics, rehabilitation, and more. We show this utility in a pilot study, sensing prediabetes, where we determined three relevant wavelengths, 470nm, 515nm, and 680nm, for glucose and created and evaluated a targeted tracking device.

ACKNOWLEDGMENTS

The authors would like to thank Xian Li for his early work in sensor selection, Hyonyoung Choi for allowing us to use his camera and photography expertise, and Kyle C. Quinn for his efforts in proofreading and editing. This research was supported in part by the National Science Foundation under grants NSF-1915398, NSF-2125561 and by the National Institute of Health under grants NIH 1R01EB029363-01 and NIH 1R01EB029767-01.

REFERENCES

[1] Nurul Akmal Binti Abd Salam, Wira Hidayat bin Mohd Saad, Zahariah Binti Manap, and Fauziyah Salehuddin. 2016. The evolution of non-invasive blood glucose monitoring system for personal application. *Journal of Telecommunication, Electronic and Computer*

Engineering (JTEC) 8, 1 (2016), 59–65.
[2] Adafruit 2022. AS7341: 11-Channel Multi-Spectral Digital Sensor. https://ams.com/documents/20143/36005/AS7341_DS000504_3-00.pdf.
[3] Mahmoud Al-Omari, Kivanc Sel, Anja Mueller, Jeffery Edwards, and Tolga Kaya. 2014. Detection of relative [Na+] and [K+] levels in sweat with optical measurements. *Journal of Applied Physics* 115, 20 (2014), 203107.
[4] M Kathleen Alam, Mark R Rohrscheib, James E Franke, Thomas M Niemczyk, John D Maynard, and M Ries Robinson. 1999. Measurement of pH in whole blood by near-infrared spectroscopy. *Applied spectroscopy* 53, 3 (1999), 316–324.
[5] Haider Ali, Faycal Bensaali, and Fadi Jaber. 2017. Novel approach to non-invasive blood glucose monitoring based on transmittance and refraction of visible laser light. *IEEE access* 5 (2017), 9163–9174.
[6] Pavel Anzenbacher Jr, Fengyu Li, and Manuel A Palacios. 2012. Toward wearable sensors: fluorescent attoreactor mats as optically encoded cross-reactive sensor arrays. *Angewandte Chemie* 124, 10 (2012), 2395–2398.
[7] Krzysztof B Beć, Justyna Grabska, and Christian W Huck. 2021. Principles and applications of miniaturized near-infrared (NIR) spectrometers. *Chemistry–A European Journal* 27, 5 (2021), 1514–1532.
[8] Matthew G Blain, Leah S Riter, Dolores Cruz, Daniel E Austin, Guangxiang Wu, Wolfgang R Plass, and R Graham Cooks. 2004. Towards the hand-held mass spectrometer: design considerations, simulation, and fabrication of micrometer-scaled cylindrical ion traps. *International Journal of Mass Spectrometry* 236, 1-3 (2004), 91–104.
[9] Karthik Budidha, Mohammad Mamouei, Nystha Baishya, Meha Qassem, Pankaj Vadgama, and Panayiotis A Kyriacou. 2020. Identification and quantitative determination of lactate using optical spectroscopy—towards a noninvasive tool for early recognition of sepsis. *Sensors* 20, 18 (2020), 5402.
[10] CareTouch 2022. CareTouch Blood Glucose Monitor Kit. https://www.amazon.com/Care-Touch-Diabetes-Testing-Kit/dp/B076VSN7TR/
[11] Albert E Cerussi, Vaya W Tanamai, David Hsiang, John Butler, Rita S Mehta, and Bruce J Tromberg. 2011. Diffuse optical spectroscopic imaging correlates with final pathological response in breast cancer neoadjuvant chemotherapy. *Philosophical transactions of the royal society A: mathematical, physical and engineering sciences* 369, 1955 (2011), 4512–4530.
[12] Charles Chabal, Louis Jacobson, Anthony J Mariano, and Edmund Chaney. 1998. Opiate abuse or undertreatment? *The Clinical Journal of Pain* 14, 1 (1998), 90–91.
[13] Vishnu Dantu, Jagannadh Vempati, and Srinivasan Srivilliputhur. 2014. Non-invasive blood glucose monitor based on spectroscopy using a smartphone. In *2014 36th annual international conference of the IEEE engineering in medicine and biology society*. IEEE, 3695–3698.
[14] ACM Dassel, R Graaff, M Sikkema, A Meijer, WG Zijlstra, and JG Aarnoudse. 1995. Reflectance pulse oximetry at the forehead improves by pressure on the probe. *Journal of clinical monitoring* 11, 4 (1995), 237–244.
[15] Digikey 2022. LED Emitters- Infrared, UV, Visible. https://www.digikey.com/en/products/filter/led-emitters-infrared-uv-visible/94
[16] Tanja Dragojević, Joseph L Hollmann, Davide Tamborini, Davide Portaluppi, Mauro Buttafava, Joseph P Culver, Federica Villa, and Turgut Durduran. 2018. Compact, multi-exposure speckle contrast optical spectroscopy (SCOS) device for measuring deep tissue blood flow. *Biomedical optics express* 9, 1 (2018), 322–334.
[17] Fatema El-Amrawy and Mohamed Ismail Nounou. 2015. Are currently available wearable devices for activity tracking and heart rate monitoring accurate, precise, and medically beneficial? *Healthcare informatics research* 21, 4 (2015), 315–320.
[18] Annika MK Enejder, Thomas G Scecina, Jeankun Oh, Martin Hunter, WeiChuan Shih, Slobodan Sasic, Gary L Horowitz, and Michael S Feld. 2005. Raman spectroscopy for noninvasive glucose measurements. *Journal of biomedical optics* 10, 3 (2005), 031114.
[19] Litong Feng, Lai-Man Po, Xuyuan Xu, Yuming Li, and Ruiyi Ma. 2014. Motion-resistant remote imaging photoplethysmography based on the optical properties of skin. *IEEE Transactions on Circuits and Systems for Video Technology* 25, 5 (2014), 879–891.
[20] Louise Finlayson, Isla RM Barnard, Lewis McMillan, Sally H Ibbotson, C Tom A Brown, Ewan Eadie, and Kenneth Wood. 2022. Depth penetration of light into skin as a function of wavelength from 200 to 1000 nm. *Photochemistry and Photobiology* 98, 4 (2022), 974–981.
[21] Rodolfo J Galindo and Grazia Aleppo. 2020. Continuous glucose monitoring: the achievement of 100 years of innovation in diabetes technology. *Diabetes research and clinical practice* 170 (2020), 108502.
[22] Mayank Goel, Eric Whitmire, Alex Mariakakis, T Scott Saponas, Neel Joshi, Dan Morris, Brian Guenter, Marcel Gavriliu, Gaetano Borriello, and Shwetak N Patel. 2015. HyperCam: hyperspectral imaging for ubiquitous computing applications. In *Proceedings of the 2015 ACM International Joint Conference on Pervasive and Ubiquitous Computing*. 145–156.
[23] Gossen 2022. Gossen MAVOSPEC BASE Innovative Spectrometer. https://www.tequipment.net/Gossen/MAVOSPEC-BASE/Light-Meters/Illuminance-Meters/.
[24] Weixi Gu, Yuxun Zhou, Zimu Zhou, Xi Liu, Han Zou, Pei Zhang, Costas J. Spanos, and Lin Zhang. 2017. SugarMate: Non-Intrusive Blood Glucose Monitoring with Smartphones. *Proc. ACM Interact. Mob. Wearable Ubiquitous Technol.* 1, 3, Article 54 (sep 2017), 27 pages.
[25] Robin Kingsley Harris. 1986. Nuclear magnetic resonance spectroscopy. (1986).
[26] Rolamjaya Hotmartua, Pujianto Wira Pangestu, Hasballah Zakaria, and Yoke Saadia Irawan. 2015. Noninvasive blood glucose detection using near infrared sensor. In *2015 International Conference on Electrical Engineering and Informatics (ICEEI)*. IEEE, 687–692.
[27] ILT350 Chroma Meter 2022. ILT350 Chroma Meter. https://www.intl-lighttech.com/products/ilt350-chroma-meter.
[28] Arvind Jina, Michael J Tierney, Janet A Tamada, Scott McGill, Shashi Desai, Beelee Chua, Anna Chang, and Mark Christiansen. 2014. Design, development, and evaluation of a novel microneedle array-based continuous glucose monitor. *Journal of diabetes science and*

technology 8, 3 (2014), 483–487.
[29] Omar S Khalil. 2004. Non-invasive glucose measurement technologies: an update from 1999 to the dawn of the new millennium. *Diabetes technology & therapeutics* 6, 5 (2004), 660–697.
[30] Svetlana Khaustova, Maxim Shkurnikov, Evgeny Tonevitsky, Viacheslav Artyushenko, and Alexander Tonevitsky. 2010. Noninvasive biochemical monitoring of physiological stress by Fourier transform infrared saliva spectroscopy. *Analyst* 135, 12 (2010), 3183–3192.
[31] Jayoung Kim, Alan S Campbell, Berta Esteban-Fernández de Ávila, and Joseph Wang. 2019. Wearable biosensors for healthcare monitoring. *Nature biotechnology* 37, 4 (2019), 389–406.
[32] Richard P Kingsborough, Alexandra T Wrobel, Devon Beck, Lauren Cantley, Shane Tysk, and Roderick Kunz. 2020. Chemical sensing via a low SWaP wearable spectrometer. In *Chemical, Biological, Radiological, Nuclear, and Explosives (CBRNE) Sensing XXI*, Vol. 11416. International Society for Optics and Photonics, 114160O.
[33] Ryan R Kroll, J Gordon Boyd, and David M Maslove. 2016. Accuracy of a wrist-worn wearable device for monitoring heart rates in hospital inpatients: a prospective observational study. *Journal of medical Internet research* 18, 9 (2016), e6025.
[34] Michele Lacerenza, Mauro Buttafava, Marco Renna, Alberto Dalla Mora, Lorenzo Spinelli, Franco Zappa, Antonio Pifferi, Alessandro Torricelli, Alberto Tosi, and Davide Contini. 2020. Wearable and wireless time-domain near-infrared spectroscopy system for brain and muscle hemodynamic monitoring. *Biomedical Optics Express* 11, 10 (2020), 5934–5949.
[35] V Lakshminarayanan and N Sriraam. 2014. The effect of temperature on the reliability of electronic components. In *2014 IEEE international conference on electronics, computing and communication technologies (CONECCT)*. IEEE, 1–6.
[36] Etienne Lareau, Frederic Lesage, Philippe Pouliot, Jerome Le Lan, Mohamad Sawan, and Dang Nguyen. 2011. Multichannel wearable system dedicated for simultaneous electroencephalography/near-infrared spectroscopy real-time data acquisitions. *Journal of biomedical optics* 16, 9 (2011), 096014.
[37] Jihyoung Lee, Kenta Matsumura, Ken-ichi Yamakoshi, Peter Rolfe, Shinobu Tanaka, and Takehiro Yamakoshi. 2013. Comparison between red, green and blue light reflection photoplethysmography for heart rate monitoring during motion. In *2013 35th Annual International Conference of the IEEE Engineering in Medicine and Biology Society (EMBC)*. 1724–1727. https://doi.org/10.1109/EMBC.2013.6609852
[38] M Lepore, M Portaccio, E De Tommasi, P De Luca, U Bencivenga, P Maiuri, and DG Mita. 2004. Glucose concentration determination by means of fluorescence emission spectra of soluble and insoluble glucose oxidase: some useful indications for optical fibre-based sensors. *Journal of Molecular Catalysis B: Enzymatic* 31, 4-6 (2004), 151–158.
[39] Huijie Li, Guangfu Wu, Zhengyan Weng, He Sun, Ravi Nistala, and Yi Zhang. 2021. Microneedle-Based Potentiometric Sensing System for Continuous Monitoring of Multiple Electrolytes in Skin Interstitial Fluids. *ACS sensors* 6, 6 (2021), 2181–2190.
[40] Linfan Li, Tsung-Chi Chen, Yue Ren, Paul I Hendricks, R Graham Cooks, and Zheng Ouyang. 2014. Mini 12, Miniature Mass Spectrometer for Clinical and Other Applications Introduction and Characterization. *Analytical chemistry* 86, 6 (2014), 2909–2916.
[41] YanFeng Li, Linda S Geiss, Nilka R Burrows, Deborah B Rolka, and Ann Albright. 2013. Awareness of prediabetes—United States, 2005–2010. *Morbidity and Mortality Weekly Report* 62, 11 (2013), 209.
[42] LibreTexts 2022. Spectroscopic Methods. https://chem.libretexts.org/@go/page/70697.
[43] Julia Madden, Conor O'Mahony, Michael Thompson, Alan O'Riordan, and Paul Galvin. 2020. Biosensing in dermal interstitial fluid using microneedle based electrochemical devices. *Sensing and Bio-Sensing Research* 29 (2020), 100348.
[44] Laxmaiah Manchikanti, Standiford Helm 2nd, Bert Fellows, Jeffrey W Janata, Vidyasagar Pampati, Jay S Grider, and Mark V Boswell. 2012. Opioid epidemic in the United States. *Pain physician* 15, 3 Suppl (2012), ES9–38.
[45] Paul D Mannheimer. 2007. The light–tissue interaction of pulse oximetry. *Anesthesia & Analgesia* 105, 6 (2007), S10–S17.
[46] Yitzhak Mendelson, R James Duckworth, and G Comtois. 2006. A wearable reflectance pulse oximeter for remote physiological monitoring. In *2006 International Conference of the IEEE Engineering in Medicine and Biology Society*. IEEE, 912–915.
[47] Ivan Moreno, Chang-Yu Tsai, David Bermúdez, and Ching-Cherng Sun. 2007. Simple function for intensity distribution from LEDs. In *Nonimaging Optics and Efficient Illumination Systems IV*, Vol. 6670. SPIE, 137–143.
[48] Deirdre Morris, Shirley Coyle, Yanzhe Wu, King Tong Lau, Gordon Wallace, and Dermot Diamond. 2009. Bio-sensing textile based patch with integrated optical detection system for sweat monitoring. *Sensors and Actuators B: Chemical* 139, 1 (2009), 231–236.
[49] Mouser 2022. Infrared Emitters. https://www.mouser.com/c/optoelectronics/infrared-data-communications/infrared-emitters/
[50] UA Müller, B Mertes, C Fischbacher, KU Jageman, and K Danzer. 1997. Non-invasive blood glucose monitoring by means of near infrared spectroscopy: methods for improving the reliability of the calibration models. *The International journal of artificial organs* 20, 5 (1997), 285–290.
[51] David M Nathan. 2015. Diabetes: advances in diagnosis and treatment. *Jama* 314, 10 (2015), 1052–1062.
[52] Ocean Insight 2022. Preconfigured Ocean FX VIS-NIR Spectrometer. https://www.oceaninsight.com/products/spectrometers/high-speed-acquisition/ocean-fx/ocean-fx-vis-nir-1/
[53] Martina O'Toole and Dermot Diamond. 2008. Absorbance based light emitting diode optical sensors and sensing devices. *Sensors* 8, 4 (2008), 2453–2479.
[54] Jakub Parak, Adrian Tarniceriu, Philippe Renevey, Mattia Bertschi, Ricard Delgado-Gonzalo, and Ilkka Korhonen. 2015. Evaluation of the beat-to-beat detection accuracy of PulseOn wearable optical heart rate monitor. In *2015 37th Annual International Conference of the*

IEEE Engineering in Medicine and Biology Society (EMBC). IEEE, 8099–8102.
[55] Pasco 2022. Spectroscopy. https://www.pasco.com/products/guides/what-is-spectroscopy
[56] Nadia K Pervez, Tanya C Garza, Michael J Gazes, James I Scholtz, Mark F Comerford, and Ioannis Kymissis. 2017. Integrated Light Management as a Path to Miniaturizing Spectrometers. In *Applied Industrial Optics: Spectroscopy, Imaging and Metrology*. ATh2A–3.
[57] David Pollreisz and Nima TaheriNejad. 2019. Detection and removal of motion artifacts in PPG signals. *Mobile Networks and Applications* (2019), 1–11.
[58] SP Preejith, Annamol Alex, Jayaraj Joseph, and Mohanasankar Sivaprakasam. 2016. Design, development and clinical validation of a wrist-based optical heart rate monitor. In *2016 IEEE International Symposium on Medical Measurements and Applications (MeMeA)*. IEEE, 1–6.
[59] Colin Raymond, Tom Matthews, and Radley M Horton. 2020. The emergence of heat and humidity too severe for human tolerance. *Science Advances* 6, 19 (2020), eaaw1838.
[60] Darren M Roblyer. 2020. Perspective on the increasing role of optical wearables and remote patient monitoring in the COVID-19 era and beyond. *Journal of Biomedical Optics* 25, 10 (2020), 102703.
[61] Roithner 2022. Roithner LaserTechnik GmbH. http://www.roithner-laser.com/
[62] Markus Rothmaier, Bärbel Selm, Sonja Spichtig, Daniel Haensse, and Martin Wolf. 2008. Photonic textiles for pulse oximetry. *Optics express* 16, 17 (2008), 12973–12986.
[63] Leah Sera and Mary Lynn McPherson. 2018. Management of opioid-induced constipation in hospice patients. *American Journal of Hospice and Palliative Medicine®* 35, 2 (2018), 330–335.
[64] Abhishek B Sharma, Leana Golubchik, and Ramesh Govindan. 2010. Sensor faults: Detection methods and prevalence in real-world datasets. *ACM Transactions on Sensor Networks (TOSN)* 6, 3 (2010), 1–39.
[65] Sanjiv Sharma, Ahmed El-Laboudi, Monika Reddy, Narvada Jugnee, Sujan Sivasubramaniyam, Mohamed El Sharkawy, Pantelis Georgiou, Desmond Johnston, Nick Oliver, and Anthony EG Cass. 2018. A pilot study in humans of microneedle sensor arrays for continuous glucose monitoring. *Analytical Methods* 10, 18 (2018), 2088–2095.
[66] Kevin AG Smet. 2020. Tutorial: The LuxPy Python toolbox for lighting and color science. *Leukos* 16, 3 (2020), 179–201.
[67] StellarRAD 2022. StellarRAD+Color Handheld-Colorimeter. https://www.shopstellarnet.com/stellarrad-color-handheld-colorimeter.
[68] Fei Teng, Timothy Cormier, Alexis Sauer-Budge, Rachita Chaudhury, Vivian E Pera, Raeef Istfan, David A Chargin, Samuel Brookfield, Naomi Yu Ko, and Darren M Roblyer. 2017. Wearable near-infrared optical probe for continuous monitoring during breast cancer neoadjuvant chemotherapy infusions. *Journal of biomedical optics* 22, 1 (2017), 014001.
[69] Hazhir Teymourian, Farshad Tehrani, Kuldeep Mahato, and Joseph Wang. 2021. Lab under the skin: microneedle based wearable devices. *Advanced healthcare materials* 10, 17 (2021), 2002255.
[70] Nikolai V Tkachenko. 2006. *Optical spectroscopy: methods and instrumentations*. Elsevier.
[71] UNLV 2022. Things you should know about photodiodes. https://www.physics.unlv.edu/~bill/PHYS483/LED_PIN.pdf
[72] Amanda Watson. 2022. Lumos. https://github.com/aawatson22/Lumos.
[73] Amanda Watson, Hyonyoung Choi, Insup Lee, and James Weimer. 2021. Raproto: an open source platform for rapid prototyping of wearable medical devices. In *Proceedings of the Workshop on Medical Cyber Physical Systems and Internet of Medical Things*. 1–6.
[74] Dominik G Wyser, Olivier Lambercy, Felix Scholkmann, Martin Wolf, and Roger Gassert. 2017. Wearable and modular functional near-infrared spectroscopy instrument with multidistance measurements at four wavelengths. *Neurophotonics* 4, 4 (2017), 041413.
[75] Jyoti Yadav, Asha Rani, Vijander Singh, and Bhaskar Mohan Murari. 2015. Prospects and limitations of non-invasive blood glucose monitoring using near-infrared spectroscopy. *Biomedical signal processing and control* 18 (2015), 214–227.
[76] LDS Yadav. 2005. Ultraviolet (UV) and visible spectroscopy. In *Organic Spectroscopy*. Springer, 7–51.
[77] Zongyin Yang, Tom Albrow-Owen, Weiwei Cai, and Tawfique Hasan. 2021. Miniaturization of optical spectrometers. *Science* 371, 6528 (2021), eabe0722.